



Aerostructural design optimization of a continuous morphing trailing edge aircraft for improved mission performance

David A. Burdette *

Gaetan K.W. Kenway †

Joaquim R. R. A. Martins‡

University of Michigan, Ann Arbor, Michigan, 48109, United States

Non-morphing, conventional aircraft wings are designed for a compromise of good performance at a variety of flight conditions. Accordingly, such wings perform sub-optimally when considered at a single flight condition. Morphing trailing edge devices offer an opportunity to change this wing design paradigm by allowing wings to adapt to varying flight conditions. This adaptability weakens the correlation between performance at various flight conditions and increases the robustness of the wing's performance, providing closer-to-optimal performance at each flight condition. To study the isolated aerodynamic effects of this increased robustness, we performed a number of aerodynamic shape optimizations of a small morphing trailing edge device at a variety of flight conditions on the Common Research Model aircraft configuration. Comparing the performance of the aircraft with a morphing region spanning the aft 10% of the wing and an aircraft without morphing demonstrated a 1.02% fuel burn reduction with the addition of the morphing for a 7,730 nmi mission. We repeated this process with the inclusion of coupled structural deformations and found a fuel burn reduction of 1.72%. This value provides a baseline for the performance improvement potential of this technology, independent of any restrictions or safety factors limiting the use of morphing trailing edge devices for maneuver or gust load alleviation.

I. Introduction

Due to its ability to add versatility to aircraft, morphing wing technology is a topic of interest for many research groups and members of the aviation industry. This increased versatility could be used for a variety of objectives, including: improving cruise efficiency, actively alleviating maneuver/gust loads, managing aeroelastic flutter, or improving maneuverability. While there are a range of morphing techniques that can achieve a variety of goals, in this work we are focused on the use of continuous morphing trailing edge devices for the purpose of improving the fuel efficiency of commercial transport sized aircraft. This technology has a relatively high market readiness level, and could help provide incremental performance increases to the conventional tube and wing configuration in the coming decades, before more unconventional configurations like the blended wing body (BWB) or truss-braced wing (TBW) reach the market. Currently, companies like Flexsys are working to develop and validate functional morphing wing devices [1, 2], to be used for new aircraft designs and for retrofitting current wings. To gain a better understanding of such devices, we examine in detail the potential continuous morphing trailing edge devices have for improving fuel burn efficiency during a typical long range commercial flight.

There has been a large amount of research done in both industry and academia considering trailing edge morphing devices. Szodruch and Hilbig [3] published a comprehensive study including analytic and experimental considerations of morphing devices for civil transport aircraft as well as military applications. Reckzeh [4] described Airbus' current approach to wing movables, and how variable camber at cruise can be used for load control. Molinari *et al.* [5, 6] explored the benefits of continuous morphing trailing edge technology using low fidelity aerodynamic models and has subsequently manufactured and tested a piezoelectric adaptive wing. Lyu and Martins [7] used high fidelity aerodynamic analysis and optimization to investigate the benefits associated with continuous morphing trailing edge technology, and found aerodynamic drag improvements of between 1 and 5% depending on how far the flight condition was from the design point. Nguyen *et al.* [8, 9, 10] have done extensive aerodynamic work studying the Variable Camber Continuous Trailing Edge Flap (VCCTEF) configuration, which uses a series of small flaps joined with an elastic material on the wing's trailing edge. Stanford [11] also studied the VCCTEF configuration. He considered flutter and maneuver alleviation, and included open loop load cases where morphing devices were not used. This

*Ph.D. Candidate, Department of Aerospace Engineering, AIAA Student Member

†Research Investigator, Department of Aerospace Engineering

‡Professor, Department of Aerospace Engineering, AIAA Associate Fellow

study brings up an important point: regulations to prevent complete failure in the event of morphing malfunction may substantially limit the benefits achieved by morphing wing technology. We consider the isolated effects of morphing wing technology resulting from improved robustness with respect to typical climb, cruise, and descent conditions. This provides us with a baseline for the efficiency improvement enabled by morphing wing technology, independent of potential restrictions on maneuver load alleviation.

The paper is organized as follows: Section II describes the computational tools used in this work. Section III defines the problem setup for the initial aerodynamic only optimizations. Section IV discusses the results of those optimizations and the fuel burn savings achieved with the morphing trailing edge. After the aerodynamic case, we consider a similar case with the addition of coupled structural deflections. Consideration of these deflections introduces larger differences between the flight conditions the aircraft experiences, increasing the incentive to improve performance robustness through morphing. The problem setup and results for that study are described in Sections V and VI, respectively. Finally, Section VII summarizes this work and suggests potential directions for future work.

II. Computational Framework

This section provides an overview of the components of the MDO for Aircraft Configurations with High fidelity (MACH) framework that were used in this work [12].

A. Geometric parametrization

Shape changes are controlled using a Free Form Deformation (FFD) approach [13], a method originating in computer graphics for efficiently producing deformations of solid body geometries [14]. The FFD method inserts the geometry of interest into a bounding box with a series of control points covering its surface. These control points define the shape of the bounding box, and deformations produced on the bounding box are interpolated onto the surface of the geometry. This approach reduces the number of shape design variables in the problem to the number of degrees of freedom of the control points. In this work, the control points are permitted movement in the z-direction only, which preserves a constant planform shape. Additional design variables (like chord, span, twist, etc.) can be added that aggregate control point deformations, giving the optimization routine a more direct path (and a gradient) towards large geometric deformations. The interpolation method used to translate FFD control point movement to deformations on the geometry produces a region of influence spanning two control points in each (i,j, and k) parametric direction and produces C^1 continuous geometries. The FFD used for the aerodynamic optimizations with a morphing region over the aft 10% of the wing is shown in Figure 1.

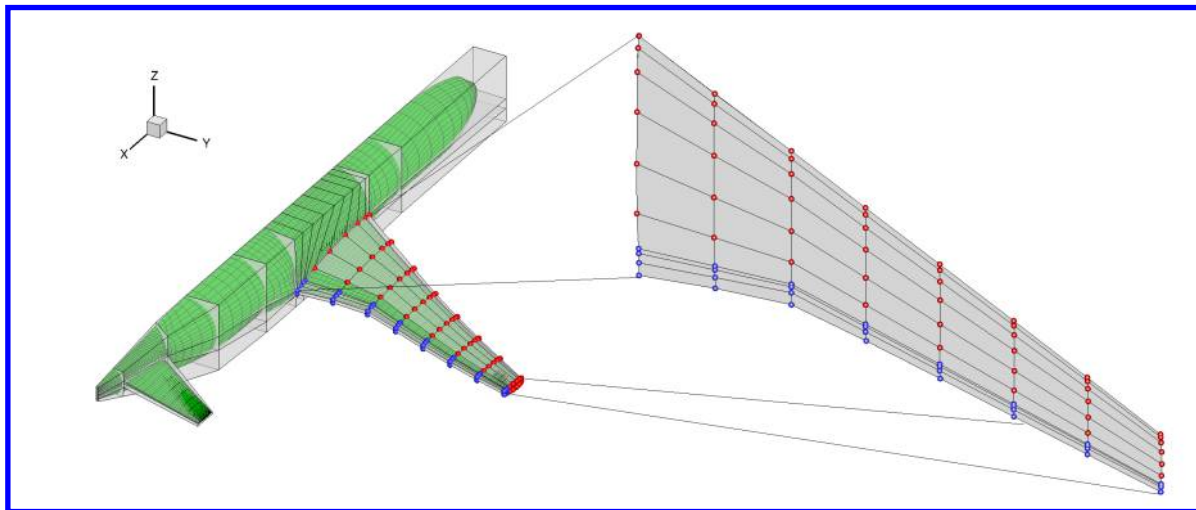


Figure 1: The control points of the FFD are shown in red and blue, where the blue control points define the morphing region used in this work.

A typical shape optimization usually uses an FFD with evenly distributed control points across its surface, but the FFD shown in Figure 1 has an uneven distribution of control points in the chord-wise direction. This chord-wise distribution was selected specifically to define the morphing region on the aft 10% of the wing. The blue control points

are located at 10, 8, 4, and 0% of the chord (from the trailing edge). Using this distribution of points, giving freedom to the aft two control points in each slice produces continuous deformations confined to the aft 10%, with a relatively small transition region providing smoothness.

The solid rotation of the tail is also controlled by the FFD. Specifically, a child FFD is defined over the tail region, with grouped control points defining the tail rotation. This tail rotation is crucial for trimming the aircraft. In previous work a child FFD placed within the parent FFD along the aft section of the wing has been used to generate trailing edge morphing. In both approaches for producing morphing, the design variables for the morphing region (whether on the parent or a child FFD) are associated with a specific flight condition. As such, the FFD provides the optimization routine with a full list of design variables, an appropriate subset of which the optimization applies to the FFD at each condition.

B. Mesh deformation

Mesh deformation for morphing trailing edge optimizations has proven to be a challenging task. The combination of low frequency span-wise structural deformations and high frequency chord-wise deformations in the morphing region often produces low quality deformed meshes. Experience has shown that an inverse-distance-weighted warping method similar to that developed by Luke *et al.* [15] can effectively warp a mesh around these types of deformations. The method interpolates deformations and rotations from the geometry surface into the volume mesh. This method produces mesh deformations that generally preserve near-perpendicularity in regions close to the geometry surface. This characteristic of the mesh warping scheme helps maintain good mesh quality around the morphing trailing edge, where many other schemes often produce mesh crossover and negative volumes. The preservation of surface perpendicularity is also beneficial for CFD calculations in and near the boundary layer. Our implementation uses an efficient search method, which helps limit the cost of the mesh movement algorithm. The mesh deformation scales with $O(\log N)$. Sensitivities are calculated with a combination of analytic and automatic differentiation (AD) methods [16].

C. CFD solver

The MACH framework's CFD solver is SUMad [17], a finite volume CFD code for structured multiblock meshes. In this work, SUMad solves the Reynolds-averaged Navier–Stokes (RANS) equations. It is important to use this level of fidelity for design of transonic wings, as small shape changes can significantly effect wave drag. A one equation Spalart–Allmaras (SA) model is used to approximate the effects of turbulence, and to close the RANS equations. Runge–Kutta (RK) and Newton–Krylov (NK) methods are used in succession to converge the flow solution. Gradients are computed with a discrete adjoint approach. The partial derivatives used in the adjoint computation are again found using analytic and automatic differentiation (AD) methods.

D. Structural solver

While the first set of results presented in this work include only aerodynamic considerations, the later results also include structural deformations, so a finite element solver is required. The MACH framework's finite element solver is the Toolkit for the Analysis of Composite Structures (TACS) [18]. TACS was designed to efficiently and accurately handle matrices with poor condition numbers, which is necessary as aircraft wing boxes modeled with shell elements yield matrices with condition numbers exceeding $O(10^9)$. Again, the adjoint method is used, producing gradient calculations which are efficient for a large number of design variables. To manage the number of structural constraints, TACS uses Kreisselmeier–Steinhauser (KS) function aggregation of stress and buckling functions.

E. Coupled aerostructural solver

SUMad and TACS are coupled in the MACH framework to obtain a static aeroelastic solution at a given flight condition. A consistent force vector is produced representing the integrated aerodynamic pressure and shear forces on the surface. These consistent forces are applied to the structural solver. Once structural deformations are solved for, they are translated from TACS to the aerodynamic surface mesh using the rigid link method like that which was introduced by Brown [19]. In this method, deformations of the aerodynamic surface mesh are taken from the nearest structural mesh node. The coupled nonlinear system of equations is solved by the aerostructural solver. Derivatives of the coupled aerostructural system are found using a coupled adjoint method [12].

F. Optimization method

The optimization routine used in this work is SNOPT (Sparse Nonlinear OPTimizer) [20]. This gradient-based optimizer is based on the sequential quadratic programming (SQP) algorithm, where the Hessian of the Lagrangian is generated using a quasi-Newton approximation. SNOPT is an efficient gradient-based optimization routine, which requires a small number of function and gradient calculations. This is important for high fidelity computations, in which function evaluations are computationally expensive. A sparse implementation of pyOpt [21] is used to interface to SNOPT through Python.

G. Mission analysis tool

The mission analysis in this work is done using pyMission [22]. This tool uses a direct transcription approach with enforcement of the governing equations at collocation points. B-splines are used to interpolate the velocity and altitude between a series of control points. pyMission offers optimization capabilities; however, that functionality is not used in this work. Rather, altitude and Mach number profiles are prescribed, and pyMission is used for analysis of the aircraft performance through an integration of an aircraft's fuel burn. A surrogate model for aircraft performance with respect to flight condition is used within pyMission to avoid an impractically large number of high fidelity function calls during the mission analysis.

H. Interpolation methods

For the aerodynamic only case where training point data is cheaper to solve for, we provide a large number of data points. For the latter aerostructural case where training point solutions are more expensive, we take steps to limit the number of training points required for the surrogate model. More details on the training point selection for the two problems are given in Sections III and V. Given the different number and distribution of training points in the two problems, two different interpolation methods are used. For the aerodynamic case, a 2-D cubic interpolant is used within the convex hull of the training points. In the aerostructural case, where a smaller number of training points that span a relatively thin region within a three dimensional space are provided, this type of interpolant yields poor performance. Instead, the regularized minimal-energy tensor-product spline (RMTS) interpolant is used [23]. This method uses cubic tensor-product splines to generate a minimum energy interpolant from unstructured data.

III. Aerodynamic problem definition

A. Baseline CRM Geometry

The baseline geometry used for the aerodynamic analyses and optimizations is the Common Research Model (CRM) wing-body-tail configuration [24, 25]. The configuration approximates a Boeing 777-200ER, and provides a thoroughly studied and understood baseline from which to start our work.

B. Mission Profile

In this section, we discuss the mission profile we used to quantify the fuel burn savings resulting from the inclusion of the morphing trailing edge. The mission has a range of 7,730 nautical miles, based on the maximum range of a Boeing 777-200ER. The mission includes two step climbs during its cruise. The step climbs are larger than what is seen in a typical flight, but the three altitudes correspond to nominal flight conditions at full fuel weight, half fuel weight, and empty fuel weight, and the inclusion of such drastic changes in flight conditions should effectively demonstrate the value of an adaptive trailing edge. The mission profile is shown in Figure 3.

The mission starts its climb at an altitude of 1500 ft. An accelerating climb continues to 10,000 ft where the indicated air speed is 250 kts. The aircraft continues climbing and increasing speed until it reaches 13,000 ft, where the velocity increase stops. At 28,000 ft, the aircraft reaches the Mach limit crossover, and becomes limited by the Mach number, which is set to 0.85. The Mach number remains at 0.85 for the remainder of the climb to the first cruise altitude of 31,000 ft, corresponding roughly to a lift coefficient of 0.5 at MTOW. The 34,000 ft altitude corresponds to a lift coefficient of 0.5 for half-fuel weight, and the final altitude of 41,000 ft gives the same lift coefficient for LGW. A slowing descent at 2° returns the aircraft to an altitude of 1,500 ft.

In Figure 3, the black points represent B-spline control points, which define the shape of the profile. That combination of control points results in the mission profile shown by the green line. The green points embedded within the green mission profile line represent the collocation points, where the governing equations are enforced by pyMission. To simplify the fuel burn calculation, approximate fuel weights are pre-defined at each of the collocation points. These

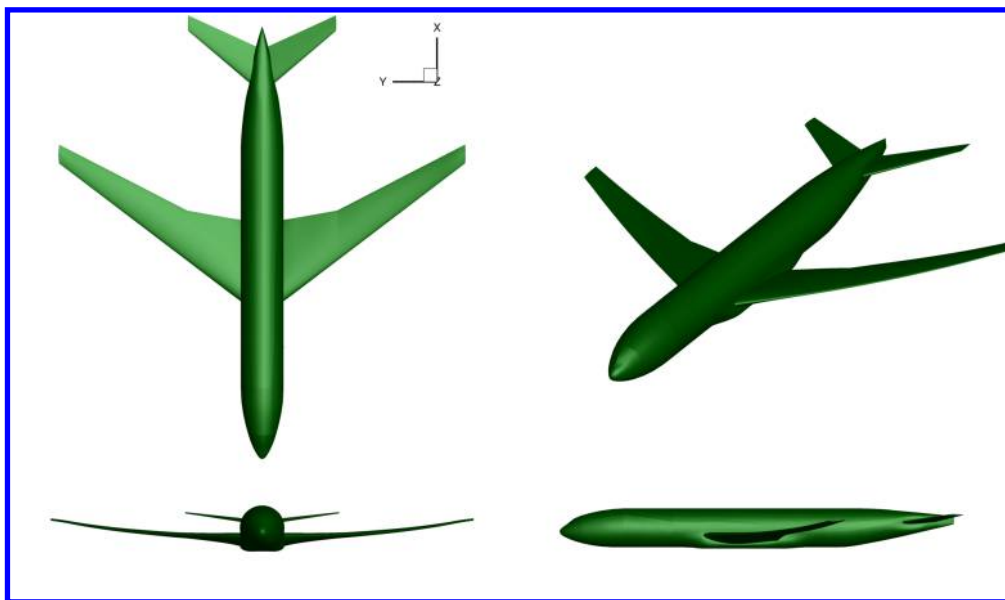


Figure 2: The CRM configuration is used as a starting point for our aerodynamic studies.

fuel weights were calculated with a lower fidelity aerodynamic panel based surrogate. This approximation neglects second order implicit effects coming from a lower drag requiring less fuel, yielding a lower required lift at points earlier in the mission. However, the first order effects resulting from a decreased drag yielding a lower fuel burn are captured.

C. Aerodynamic surrogate model

During the mission analysis, an aerodynamic surrogate is required to prevent the mission analysis from becoming unreasonably slow. The computational cost of a high fidelity RANS solution is too large for use at every flight condition encountered by the mission analysis tool during its convergence. As such, we provide aerodynamic performance through a surrogate model that can be evaluated quickly. The data for these analyses is a series of trimmed lift-to-drag ratios computed at a variety of points, as shown in Figure 4. Once the L/D values are computed, the surrogate is constructed with a cubic interpolation function, along with a nearest point approximation for points that fall outside the convex hull of the training data. Because we are considering only aerodynamic effects in this case, a two dimensional flight condition space is sufficient, assuming that the Reynolds number changes are small. This will not be the case in the later aerostructural study, where structural deflections are a function of the additional dimension.

D. Optimization problem formulation

The objective of this study is to develop an adaptive morphing trailing edge wing that outperforms a conventional wing in terms of fuel burn over the provided mission. Starting from the baseline CRM configuration, a series of 240 aerodynamic shape optimizations at the various flight conditions shown in Figure 4 are performed. The purpose of these optimizations is to find the shape of the morphing section that provides the best performance for the wing at the given flight conditions. By aggregating the performance improvements resulting from wing morphing at each of the flight conditions, we can quantify the fuel burn reduction provided by adaptive wing technology.

The problem definition for each of the 240 aerodynamic shape optimizations is identical, except for the variance in flight conditions. Thirty-two morphing design variables were used in each optimization. Tail rotation and angle of attack are also variables, to allow the aircraft to trim and meet its lift requirement. A wing volume constraint is used to ensure that sufficient volume is available in the wing for fuel. Additionally, to ensure that the optimized shapes are practical, 200 linear thickness constraints are distributed throughout the morphing section of the wing. These constraints allow a 2% increase or decrease in thickness. Without this small freedom, the problem becomes too strictly constrained, and the optimizer is unable to consistently find feasible solutions at the various flight conditions we have considered. A more detailed explanation of the optimization problems used to define optimal trailing edge shapes with

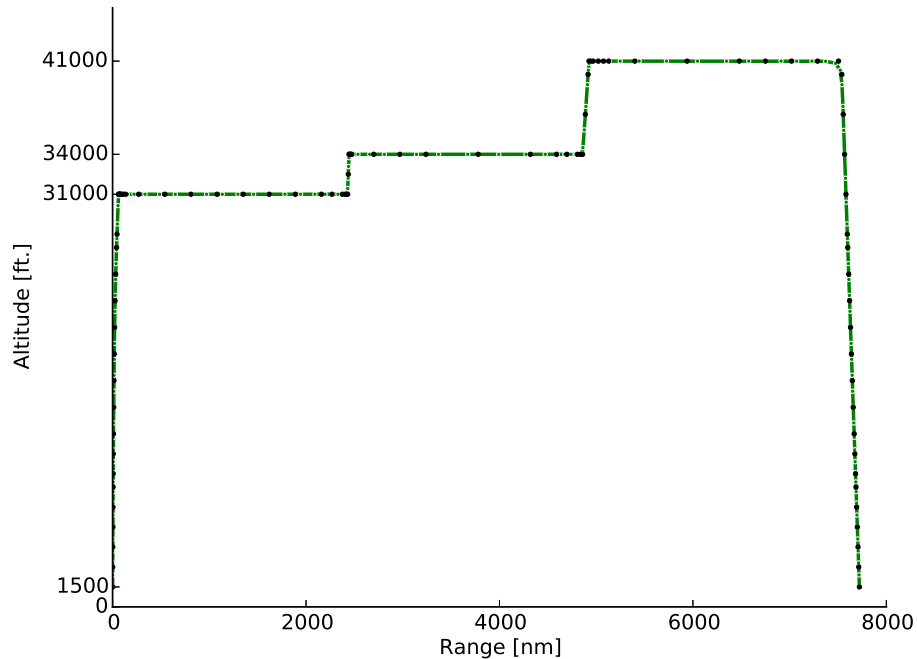


Figure 3: The representative mission used in the morphing trailing edge aerodynamic optimization includes climb, cruise (with two step climbs), and descent.

respect to flight conditions is given in Table 1.

	Function/variable	Description	Quantity
minimize	C_D	Drag coefficient	
with respect to	α	Angle of attack	1
	x_{shape}	Morphing region FFD control points	32
	η	Tail rotation angle	1
		Total design variables	34
subject to	$C_L = C_L^*$	Lift coefficient constraint	1
	$C_{M_y} = 0$	Moment coefficient	1
	$V/V_{\text{init}} \geq 1$	Fuel volume	1
	$0.98 \geq t/t_{\text{init}} \geq 1.02$	Thickness constraints	200
		Total constraints	203

Table 1: Overview of a morphing trailing edge optimization problem.

IV. Mission performance with an aerodynamically optimized adaptive trailing edge

A. Aerodynamic shape optimization results

The aerodynamic shape optimizations were completed with a 363,000 cell (L2) mesh. A 3 million cell (L1) mesh was then used for an aerodynamic analysis of the baseline wing at each of the stencil points. Next, the drag reduction between the L1 and L2 meshes for the baseline wing at each flight condition was computed. This drag reduction was then applied to the results from the morphing shape optimizations, to give an appropriate estimate of the drag on the morphed designs throughout the stencil. This approach prevents the need for any optimization to take place on the

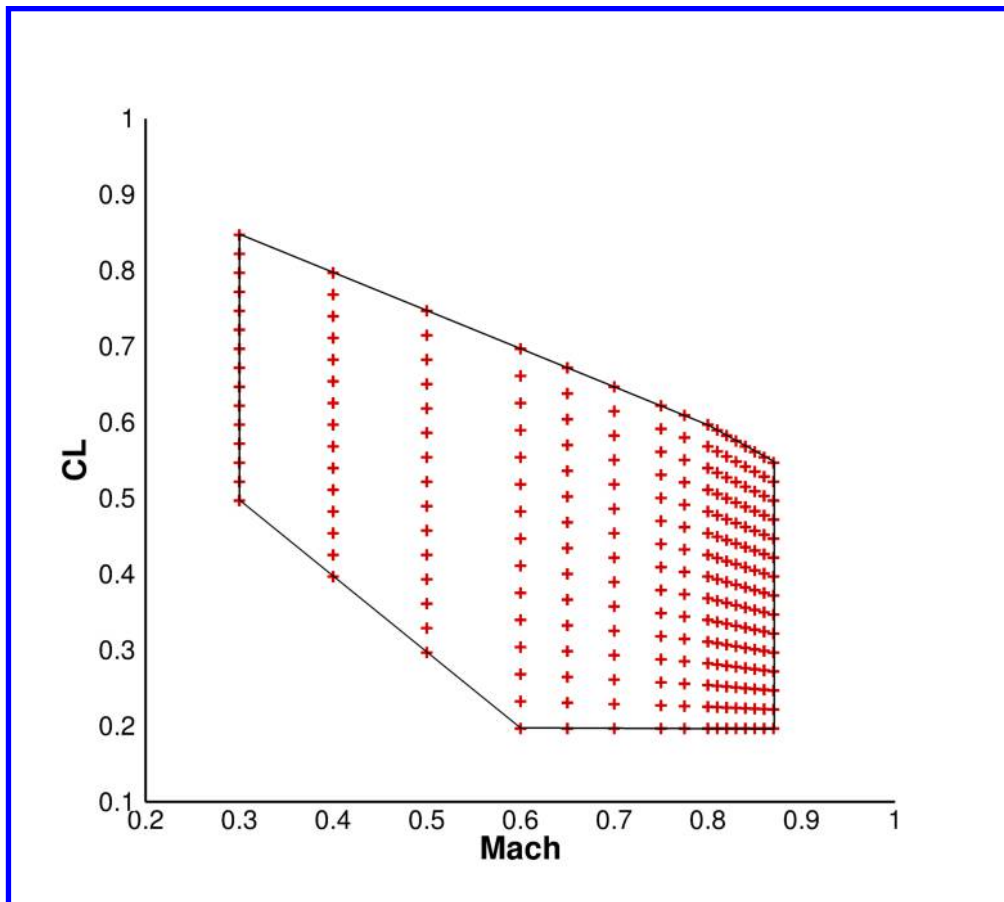


Figure 4: A 240-point stencil was used to create surrogates of the aerodynamic performance.

finer mesh, saving computational time [26]. The approach is summarized as follows:

$$D_{1m} = D_{1b} - D_{2b} + D_{2m}$$

where D_{1m} is the drag coefficient on the morphing trailing edge wing with the L1 mesh, D_{1b} is the drag coefficient on the baseline wing with the L1 mesh, D_{2m} is the drag coefficient on the morphing trailing edge wing with the L2 mesh, and D_{2b} is the drag coefficient on the baseline wing with the L2 mesh.

The purpose of these optimizations is to create an aerodynamic surrogate for mission analysis, so we consider the results of the optimizations within that context. To visualize the impact of the adaptive trailing edge on the aircraft's performance, we consider the difference in drag predicted throughout the stencil by the two surrogates, as shown in Figure 5.

By analyzing the drag reduction plotted in Figure 5, we see that through a large region of the stencil, the drag reduction is less than 1%. However, near the boundaries of the stencil we see drag reductions as large as 5%. This result makes sense, because in the region where there is little savings, the Mach number and lift coefficient are both relatively low. This means that the wave drag and induced drag are low, and the adaptive trailing edge cannot reduce them much more. In the regions with larger Mach number or lift coefficient, the drag reduced more, as those off-design conditions produce more extraneous drag that can be removed. While the baseline configuration shows strong performance robustness, particularly as compared to a wing designed with single or multipoint optimization near cruise, the addition of the morphing trailing edge is able to provide additional performance improvements at off-design conditions.

For an example of how these savings are actually achieved, we consider in more detail one of the morphing trailing edge results, as shown in Figure 6. At this point, the drag coefficient is reduced by 4.62%. We can see this is a result of reduced wave drag and induced drag, as the shock (shown in red) has become smaller and the lift distribution is closer

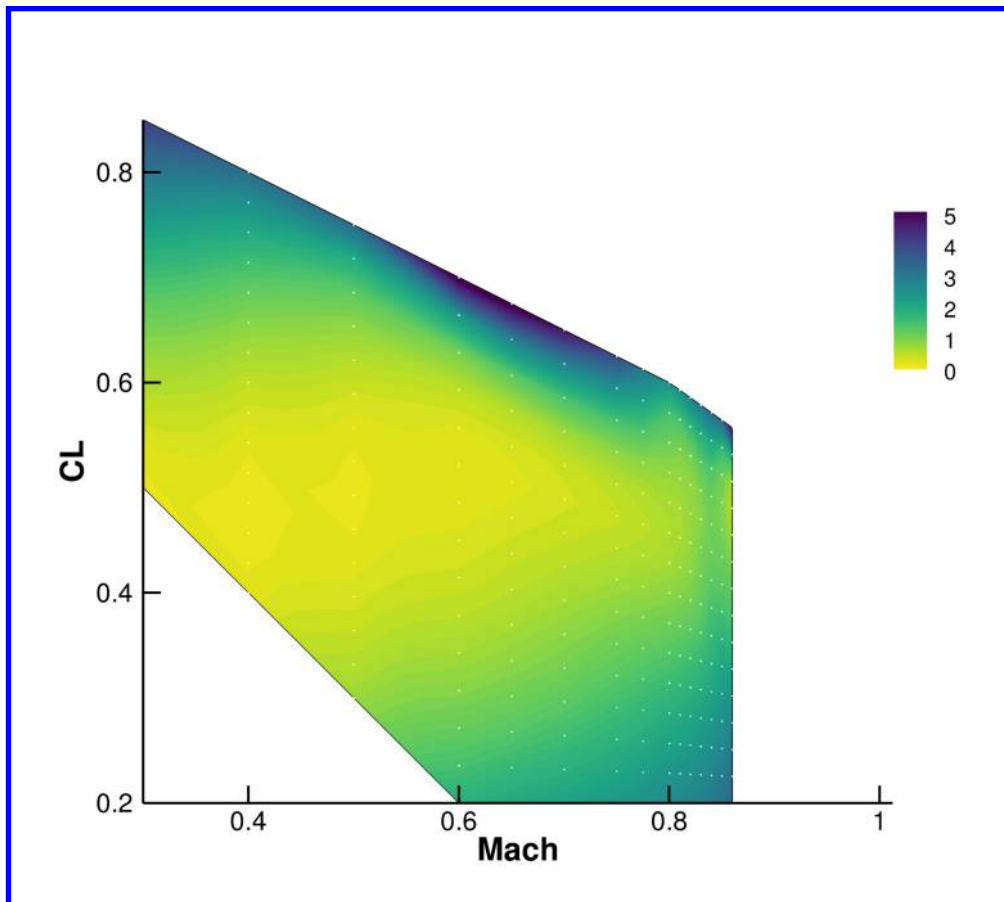


Figure 5: The percentage drag reduction throughout the stencil between the baseline CRM and the wing with an adaptive morphing trailing edge.

to elliptical after the morphing. On the right side of Figure 6, we also see airfoil and pressure distribution slices taken from four spanwise locations labelled A through D in the planform view. These slices also have an enlarged view of the morphing region, and the shapes that are achieved with the FFD parametrization we have used.

B. Mission performance of an adaptive wing

While the drag improvements are insightful, the true objective of this study is to reduce fuel burn over the course of the example mission, so we now consider what effects the trailing edge has in that regard. A summary of the fuel burn for the optimized wing and the original CRM is given in Table 2.

Wing	Fuel Weight [lbs]	Percent Reduction
Nominal CRM	105,737	-
Morphing trailing edge	104,639	1.04

Table 2: The adaptive trailing edge reduces the fuel burn by more than 1% as compared to the baseline wing.

As we can see from Table 2, the drag reductions achieved by the adaptive trailing edge successfully reduced the fuel burn by more than 1%. This is a relatively modest fuel burn improvement, but it is important to keep in mind what has been considered in this analysis, and conversely, what has not. This performance improvement is a result of an analysis in which the effects from increased aerodynamic robustness provided by the morphing trailing edge have been isolated. This improvement is strictly a result of improved aerodynamic performance during the climb, cruise, and descent portions of a typical range mission for an aircraft of this size. This result illustrates a rigid wing's weakness in performing at a range of flight conditions experienced during a typical mission, as well as the ability of

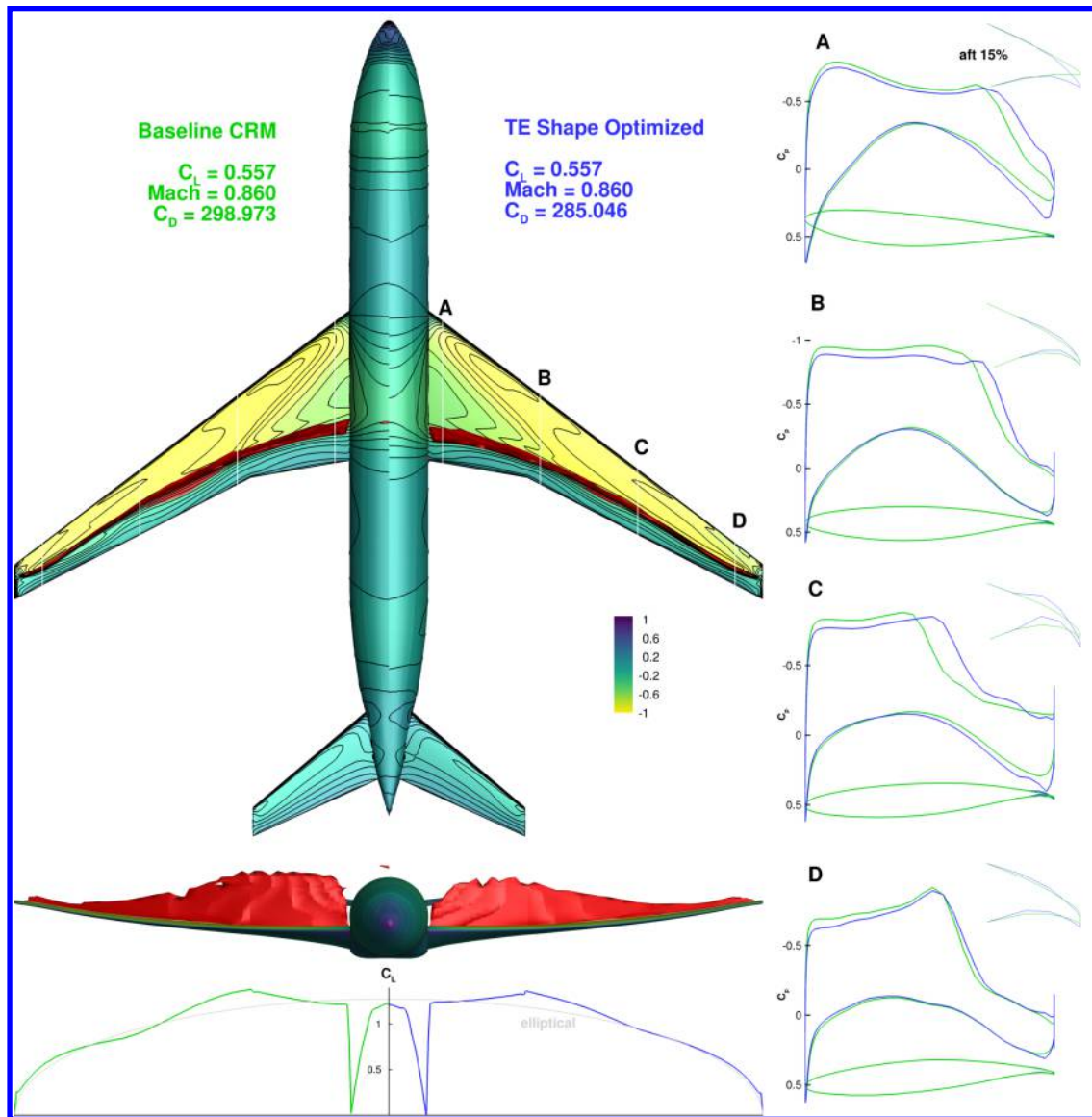


Figure 6: A summary of the morphing trailing edge aerodynamic shape optimization at $M = 0.86$ and $C_L = 0.557$.

a small morphing trailing edge device on the aft 10% of the wing to effectively manage that weakness and improve the aircraft's robustness. We now continue our study, and consider the effects of structural deformations during the mission.

V. Coupled aerostructural problem definition

A. Baseline uCRM Geometry

The baseline configuration for the aerostructural cases is the undeformed Common Research Model (uCRM) [27]. This configuration provides a jig shape and structure that deforms to the the shape of the original CRM at 1 g. The jig shape was found using an inverse design procedure. Using this procedure Kenway *et al.* [27] produced a wing whose drag is within 1 drag count of the original CRM at the design point, and can be accurately structurally deformed at other flight conditions.

B. Mission Profile

In this aerostructural analysis, we use essentially the same mission profile as was used in the aerodynamic analysis, but a few details of the mission become more important with the inclusion of structural considerations. First, because we

are including structural deformations, the constant Reynolds number approximation is no longer valid. To compensate, we prescribe the altitude at each flight condition as well as the Mach number and lift coefficient. This gives us the three-dimensional flight condition space, which is discussed in more detail in the next section. The increased dimensionality of the flight condition space did affect the selection of the mission profile. By selecting a mission in which the Mach number is a function of altitude, we reduce the dimensionality of the space the surrogate model needs to represent, allowing the use of fewer training data points. As such, the Mach number profile during descent does not exactly match that seen during a typical mission, but the effects of this difference are small with respect to the mission performance. Note also that this assumption was used during the aerodynamic only study, to make the two studies as similar as possible and comparable. The mission profile and the altitude-Mach number relationship used to generate it can be seen in Figure 7.

C. Surrogate Model

This mission profile was tested using pyMission and a low fidelity performance surrogate developed with MACH's panel method code, Tripan [28]. An approximate lift coefficient profile required to fly the mission with the CRM was developed. This distribution served as the starting point from which the higher fidelity surrogate model's training points were selected. Given that the altitude-Mach number relation is prescribed throughout the mission, it can also be prescribed for the training data. However, variations are required in the other two dimensions. The relationship between the low fidelity data and the location of the training points can be seen in Figure 7. The low fidelity mission data is shown in black, while the selected training data points are shown in red. Note that like in the aerodynamic only case, training points are more clustered near the transonic cruise region, where performance gradients are much larger than those in subsonic and lower lift regions. While the relationship between Mach number and altitude would have allowed the surrogate model to be reduced to two dimensions, that simplification is not made. The additional computational time required to converge the RMTS interpolant with a third dimension as compared to just two dimensions was negligible, so the simplification was not necessary.

D. Optimization problem formulation

Starting from the baseline uCRM, we perform 65 optimizations of the morphing trailing edge shape. The optimization formulation is essentially identical to that from the aerodynamic only study, however structural deflections at each flight condition are included. In typical aerodynamic shape optimizations there are no considerations of structural effects, while typical aerostructural optimizations typically include control over both the structural sizing and the OML shape. This optimization does not fall strictly into either of those typical categories, as here there are no structural design variables. We are performing aerodynamic shape optimization with coupled structural analysis. The optimization problem is outlined in Table 3.

	Function/variable	Description	Quantity
minimize	C_D	Drag coefficient	
with respect to	α	Angle of attack	1
	x_{shape}	Morphing region FFD control points	32
	η	Tail rotation angle	1
		Total design variables	34
subject to	$C_L = C_L^*$	Lift coefficient constraint	1
	$C_{M_y} = 0$	Moment coefficient	1
	$V/V_{\text{init}} \geq 1$	Fuel volume	1
	$0.98 \geq t/t_{\text{init}} \geq 1.02$	Thickness constraints	200
		Total constraints	203

Table 3: Overview of a morphing trailing edge optimization problem including structural deformations.

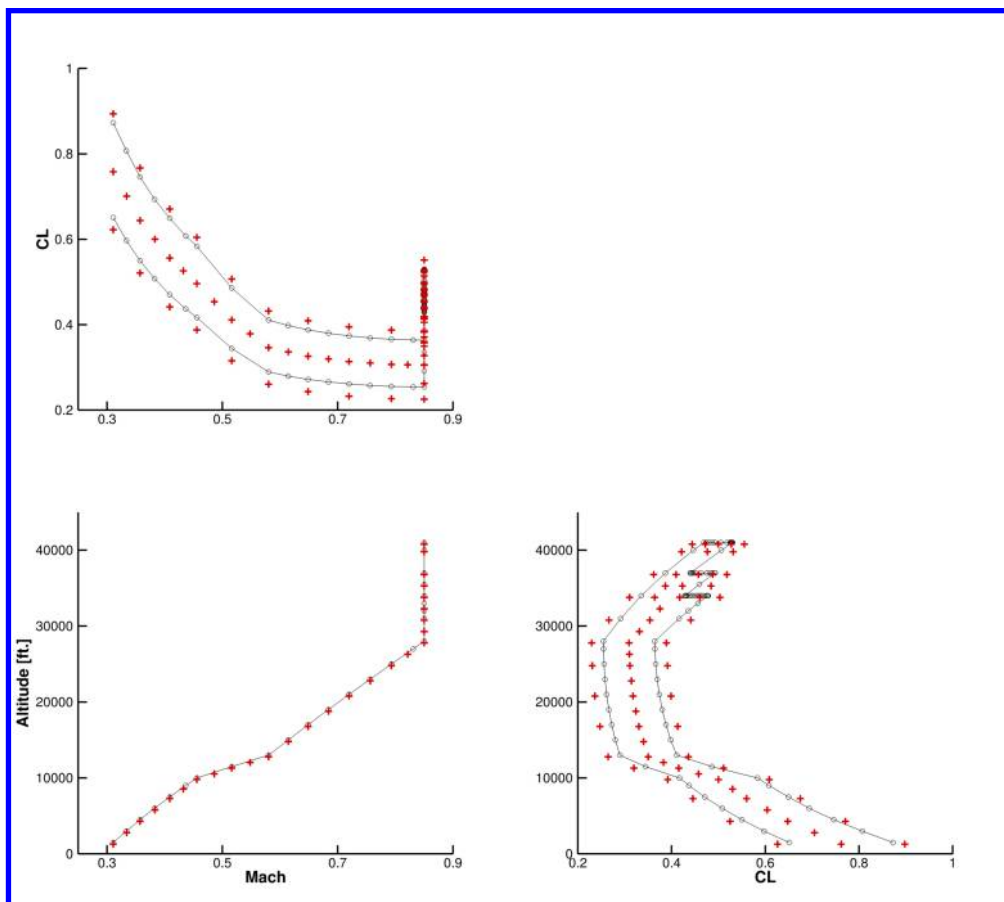


Figure 7: A set of 65 training points (in red) were used in the aerostructural performance surrogate. The training point locations were selected based on a low fidelity mission analysis model, shown in black.

VI. Mission performance with an aerostructurally optimized adaptive trailing edge

A. Coupled aerostructural optimization of the trailing edge shape

As we did for the aerodynamic results, we first consider the drag reduction resulting from the addition of the morphing trailing edge. The percentage drag reduction is shown in Figure 8. Note that this is not the exact interpolant used for the mission analysis, but rather a simplified two dimensional surrogate that takes advantage of the relationship between altitude and Mach number. This simplified interpolant was plotted instead, as the visualization of an interpolant is much easier in two dimensions than it is in three. Because this is the simplified interpolant, it is important to note that altitude changes also include changes in Mach number, as defined in Figure 7. The white points superimposed over the contour show the locations of the training data. While the interpolant solves for minimal energy throughout the entire region shown, values outside the convex hull of the training data should not be considered accurate. The energy-minimizing approach of this interpolant yields poor results in regions extrapolating from the provided data. However, as the data we need lies within the training data, this is not a problem.

Within the region of interest, the contour shows similar results to those seen in Figure 5 for the aerodynamic case. First, we see that as the altitude and Mach number are increased, the savings from the addition of the morphing trailing edge are also increased. We also see increased savings at the larger lift coefficients, although this trend is not as strong as it was in the aerodynamic case. With the inclusion of altitude variation, the flight conditions with high lift coefficients are all at low altitude, which has reduced the savings from the morphing trailing edge. While the reductions at the low altitude conditions are smaller than they were for the aerodynamic case, they are larger almost everywhere else in the mission. This suggests that the benefits of a morphing trailing edge are more substantial with the inclusion of structural deflections.

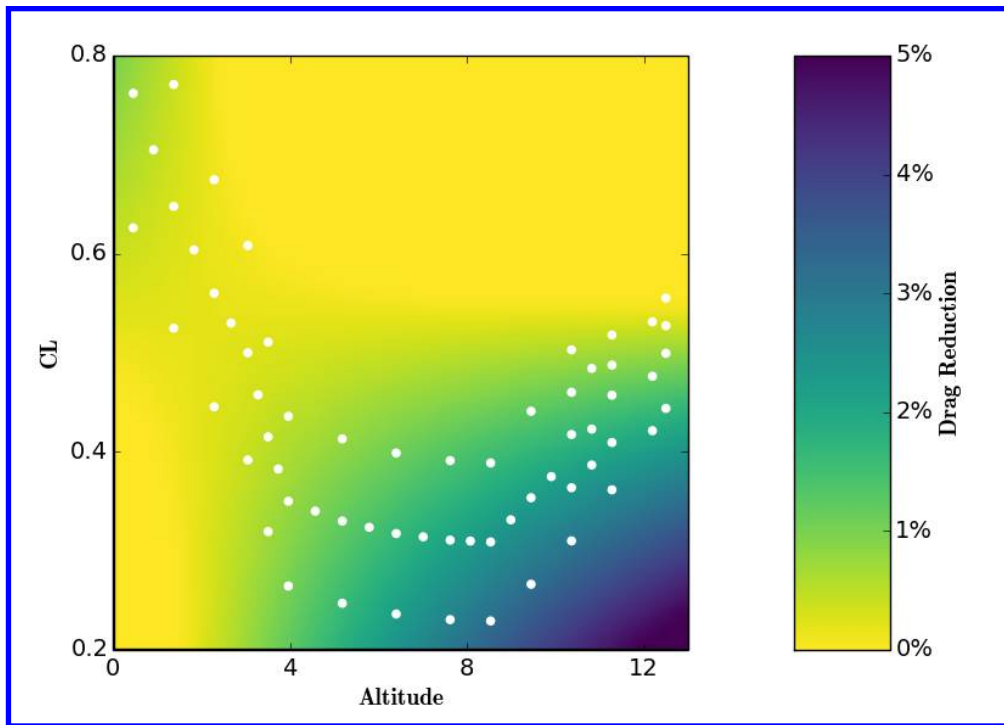


Figure 8: The percentage drag reduction for a 2-D interpolation of the aerostructural morphing trailing edge data.

B. Mission performance of an adaptive wing including structural deflections

Again, the true objective of these studies is to find the fuel burn improvements provided by the adaptive morphing trailing edge. With performance surrogates for both the baseline uCRM and the uCRM retrofitted with a morphing trailing edge on the aft 10% of the wing, we computed the fuel burn for each configuration over the prescribed mission. The fuel burn results are shown in Table 4.

Wing	Fuel Weight [lbs]	Percent Reduction
Nominal uCRM	100,568	-
Morphing Trailing Edge	98,834	1.72

Table 4: The adaptive trailing edge reduces the fuel burn by 1.72% compared to the baseline uCRM.

From the results in Table 4, we can see that with the addition of structural deformations, use of a morphing trailing edge reduced the fuel burn by 1.72%. This is a substantial increase compared to the 1.04% seen for the aerodynamic only case. It is again important to consider what is responsible for that savings. The additional fuel burn reduction is strictly a result of the addition of structural deflections throughout the mission. The consideration of structural deflections applies a wider range of conditions to the wing throughout the mission, resulting in a larger potential for savings from increased robustness.

VII. Conclusions and future work

To study how impactful the increased performance robustness offered by morphing trailing edge technology is on an aircraft's fuel burn, we performed a series of aerodynamic and aerostructural optimizations of morphing trailing edge shapes. Using the performance characteristics of wings with and without a morphing trailing edge, assembled into surrogate models, we performed a number of mission analyses to compute the fuel burn of the various configurations. In the aerodynamic only case where the wing had a rigid structural shape, a 1.02% fuel burn reduction was achieved with the addition of a morphing trailing edge. After adding coupled structural deflections to the aerodynamic optimizations of the trailing edge shapes, the fuel burn was reduced by 1.72% compared to the baseline uCRM.

These results clearly demonstrate that a retrofitted morphing trailing edge device distributed over the aft 10% of an aircraft's wing has the potential to substantially improve the aircraft's performance robustness. This improved robustness manifests itself as fuel burn reductions of 1–2%, depending on a number of conditions, including the original configuration, and the mission being flown. In these studies, the fuel burn savings are strictly a result of increased performance during typical flight conditions. Additional savings from maneuver and gust load alleviation were not considered. By isolating the effects of the improved robustness, we provide a baseline for the fuel burn savings, which is independent of the extent to which regulations allow morphing enabled MLA. In previous work, the authors have shown that maneuver load alleviation with a morphing device on the aft 40% of a wing can produce structural weight reductions of up to 25% [29]. This additional benefit of morphing devices offers the potential for additional fuel burn savings of up to 5% on the mission used in these analyses. However, this reduction is limited by a currently undetermined additional safety factor applied to morphing-enabled maneuver and gust load alleviation. With this analysis, we see that even without any permitted structural sizing reductions enabled by morphing, fuel burn savings of 1–2% are available from the increased performance robustness offered by the morphing trailing edge. Any additional savings from lightening the structure would add to this baseline reduction. In future work we plan to examine the coupled effect such structural reductions have on the effectiveness of the morphing device during a mission, as increasing a wing's flexibility potentially strengthens the relationship between improved robustness and decreased fuel burn.

VIII. Acknowledgements

The authors extend their gratitude to Dr. Fay Collier, who supported this work through award No. NNX14AC73A. This work used the Extreme Science and Engineering Discovery Environment (XSEDE), which is supported by National Science Foundation grant number ACI-1053575 [30]. The authors would also like to recognize Dr. John Hwang for his work on and assistance with the RMTS interpolant.

References

- [1] Kota, S., Hetrick, J., Osborn, R., Paul, D., Pendleton, E., Flick, P., and Tilmann, C., "Design and Application of Compliant Mechanisms for Morphing Aircraft Structures," *Proceedings of SPIE*, Vol. 5054, 2003, p. 25.
- [2] Kota, S., Osborn, R., Ervin, G., Maric, D., Flick, P., and Paul, D., "Mission Adaptive Compliant Wing—Design, Fabrication and Flight Test," *RTO Applied Vehicle Technology Panel (AVT) Symposium*, 2009.
- [3] Szodruch, J. and Hilbig, R., "Variable Wing Camber for Transport Aircraft," *Progress in Aerospace Sciences*, Vol. 25, 1998, pp. 297–328.
- [4] Reckzeh, D., "MULTIFUNCTIONAL WING MOVEABLES: DESIGN OF THE A350XWB AND THE WAY TO FUTURE CONCEPTS," .
- [5] Molinari, G., Quack, M., Dmitriev, V., Morari, M., Jenny, P., and Ermanni, P., "Aero-Structural Optimization of Morphing Airfoils for Adaptive Wings," *Journal of Intelligent Material Systems and Structures*, Vol. 22, No. 10, 2011, pp. 1075–1089. doi:[10.1177/1045389X11414089](https://doi.org/10.1177/1045389X11414089).
- [6] Molinari, G., Quack, M., Arrieta, A. F., Morari, M., and Ermanni, P., "Design, realization and structural testing of a compliant adaptable wing," *Smart Materials and Structures*, Vol. 24, No. 10, 2015, pp. 105027.
- [7] Lyu, Z. and Martins, J. R. R. A., "Aerodynamic Shape Optimization of an Adaptive Morphing Trailing Edge Wing," *Journal of Aircraft*, Vol. 52, No. 6, November 2015, pp. 1951–1970. doi:[10.2514/1.C033116](https://doi.org/10.2514/1.C033116).
- [8] Urnes, J., Nguyen, N., Ippolito, C., Totah, J., Trinh, K., and Ting, E., "A Mission Adaptive Variable Camber Flap Control System to Optimize High Lift and Cruise Lift to Drag Ratios of Future N+ 3 Transport Aircraft," *51st AIAA Aerospace Sciences Meeting, Grapevine, TX*, 2013.
- [9] Kaul, U. K. and Nguyen, N. T., "Drag Optimization Study of Variable Camber Continuous Trailing Edge Flap (VCCTEF) Using OVERFLOW," *AIAA Paper*, Vol. 2444, 2014.
- [10] Ting, E., Dao, T., and Nguyen, N., "Aerodynamic Load Analysis of a Variable Camber Continuous Trailing Edge Flap System on a Flexible Wing Aircraft," *AIAA SciTech Conference*, 2015, pp. 5–9.
- [11] Stanford, B., "Static and Dynamic Aeroelastic Tailoring with Variable Camber Control," *15th Dynamics Specialists Conference*, 2016, p. 1097.
- [12] Kenway, G. K. W., Kennedy, G. J., and Martins, J. R. R. A., "Scalable Parallel Approach for High-Fidelity Steady-State Aeroelastic Analysis and Derivative Computations," *AIAA Journal*, Vol. 52, No. 5, May 2014, pp. 935–951. doi:[10.2514/1.J052255](https://doi.org/10.2514/1.J052255).
- [13] Kenway, G. K., Kennedy, G. J., and Martins, J. R. R. A., "A CAD-Free Approach to High-Fidelity Aerostructural Optimization," *Proceedings of the 13th AIAA/ISSMO Multidisciplinary Analysis Optimization Conference*, Fort Worth, TX, Sept. 2010, AIAA 2010-9231.
- [14] Sederberg, T. W. and Parry, S. R., "Free-form Deformation of Solid Geometric Models," *SIGGRAPH Comput. Graph.*, Vol. 20, No. 4, Aug. 1986, pp. 151–160. doi:[10.1145/15886.15903](https://doi.org/10.1145/15886.15903).
- [15] Luke, E., Collins, E., and Blades, E., "A fast mesh deformation method using explicit interpolation," *Journal of Computational Physics*, Vol. 231, No. 2, 2012, pp. 586–601.
- [16] Martins, J. R. R. A. and Hwang, J. T., "Review and Unification of Methods for Computing Derivatives of Multidisciplinary Computational Models," *AIAA Journal*, Vol. 51, No. 11, November 2013, pp. 2582–2599. doi:[10.2514/1.J052184](https://doi.org/10.2514/1.J052184).
- [17] van der Weide, E., Kalitzin, G., Schluter, J., and Alonso, J. J., "Unsteady Turbomachinery Computations Using Massively Parallel Platforms," *Proceedings of the 44th AIAA Aerospace Sciences Meeting and Exhibit*, Reno, NV, 2006, AIAA 2006-0421.
- [18] Kennedy, G. J. and Martins, J. R. R. A., "A Parallel Finite-Element Framework for Large-Scale Gradient-Based Design Optimization of High-Performance Structures," *Finite Elements in Analysis and Design*, Vol. 87, September 2014, pp. 56–73. doi:[10.1016/j.finel.2014.04.011](https://doi.org/10.1016/j.finel.2014.04.011).
- [19] Brown, S. A., "Displacement Extrapolation for CFD+CSM Aeroelastic Analysis," *Proceedings of the 35th AIAA Aerospace Sciences Meeting*, Reno, NV, 1997, AIAA 1997-1090.
- [20] Gill, P. E., Murray, W., and Saunders, M. A., "SNOPT: An SQP algorithm for large-scale constrained optimization," *SIAM Journal of Optimization*, Vol. 12, No. 4, 2002, pp. 979–1006. doi:[10.1137/S1052623499350013](https://doi.org/10.1137/S1052623499350013).
- [21] Perez, R. E., Jansen, P. W., and Martins, J. R. R. A., "pyOpt: A Python-Based Object-Oriented Framework for Nonlinear Constrained Optimization," *Structural and Multidisciplinary Optimization*, Vol. 45, No. 1, January 2012, pp. 101–118. doi:[10.1007/s00158-011-0666-3](https://doi.org/10.1007/s00158-011-0666-3).
- [22] Kao, J. Y., Hwang, J. T., Martins, J. R. R. A., Gray, J. S., and Moore, K. T., "A Modular Adjoint Approach to Aircraft Mission Analysis and Optimization," *Proceedings of the AIAA Science and Technology Forum and Exposition (SciTech)*, Kissimmee, FL, January 2015, AIAA 2015-0136.
- [23] Hwang, J. T. and Martins, J. R. R. A., "A fast, robust interpolant for scattered multivariate data using regularized minimal-energy tensor-product splines," *ACM Transactions on Mathematical Software*, 2016.

- [24] Vassberg, J. C., DeHaan, M. A., Rivers, S. M., and Wahls, R. A., "Development of a Common Research Model for Applied CFD Validation Studies," 2008, AIAA 2008-6919.
- [25] Chen, S., Lyu, Z., Kenway, G. K. W., and Martins, J. R. R. A., "Aerodynamic Shape Optimization of the Common Research Model Wing-Body-Tail Configuration," *Journal of Aircraft*, Vol. 53, No. 1, January 2016, pp. 276–293. doi:[10.2514/1.C033328](https://doi.org/10.2514/1.C033328).
- [26] Lyu, Z., Kenway, G. K. W., and Martins, J. R. R. A., "Aerodynamic Shape Optimization Investigations of the Common Research Model Wing Benchmark," *AIAA Journal*, Vol. 53, No. 4, apr 2015, pp. 968–985. doi:[10.2514/1.j053318](https://doi.org/10.2514/1.j053318).
- [27] Kenway, G. K. W., Kennedy, G. J., and Martins, J. R. R. A., "Aerostructural Optimization of the Common Research Model Configuration," *15th AIAA/ISSMO Multidisciplinary Analysis and Optimization Conference*, Atlanta, GA, June 2014, AIAA 2014-3274.
- [28] Kennedy, G. J. and Martins, J. R. R. A., "A parallel aerostructural optimization framework for aircraft design studies," *Structural and Multidisciplinary Optimization*, Vol. 50, No. 6, December 2014, pp. 1079–1101. doi:[10.1007/s00158-014-1108-9](https://doi.org/10.1007/s00158-014-1108-9).
- [29] Burdette, D. A., Kenway, G. K., and Martins, J. R. R. A., "Performance Evaluation of a Morphing Trailing Edge Using Multipoint Aerostructural Design Optimization," *57th AIAA/ASCE/AHS/ASC Structures, Structural Dynamics, and Materials Conference*, American Institute of Aeronautics and Astronautics, January 2016. doi:[10.2514/6.2016-0159](https://doi.org/10.2514/6.2016-0159).
- [30] Towns, J., Cockerill, T., Dahan, M., Foster, I., Gaither, K., Grimshaw, A., Hazlewood, V., Lathrop, S., Lifka, D., Peterson, G. D., Roskies, R., Scott, J. R., and Wilkens-Diehr, N., "XSEDE: Accelerating Scientific Discovery," *Computing in Science and Engineering*, Vol. 16, No. 5, 2014, pp. 62–74. doi:[10.1109/MCSE.2014.80](https://doi.org/10.1109/MCSE.2014.80).

This article has been cited by:

1. Nicolas Bons, Xiaolong He, Charles A. Mader, Joaquim Martins. Multimodality in Aerodynamic Wing Design Optimization .
[\[Citation\]](#) [\[PDF\]](#) [\[PDF Plus\]](#)